Study of fission gas products effect on thermal hydraulics of the WWER1000 with enhanced subchannel method

Majid Bahonar[1] and Mahdi Aghaie[*2]

[1]*Department of Nuclear Engineering, Science and Research Branch, Islamic Azad University, Tehran, Iran*
[2]*Department of Engineering, Shahid Beheshti University, G.C, P.O.Box 1983963113, Tehran, Iran*

Abstract. Thermal hydraulic (TH) analysis of nuclear power reactors is utmost important. In this way, the numerical codes that preparing TH data in reactor core are essential. In this paper, a subchannel analysis of a Russian pressurized water reactor (WWER1000) core with enhanced numerical code is carried out. For this, in fluid domain, the mass, axial and lateral momentum and energy conservation equations for desired control volume are solved, numerically. In the solid domain, the cylindrical heat transfer equation for calculation of radial temperature profile in fuel, gap and clad with finite difference and finite element solvers are considered. The dependence of material properties to fuel burnup with Calza-Bini fuel-gap model is implemented. This model is coupled with Isotope Generation and Depletion Code (ORIGEN2.1). The possibility of central hole consideration in fuel pellet is another advantage of this work. In addition, subchannel to subchannel and subchannel to rod connection data in hexagonal fuel assembly geometry could be prepared, automatically. For a demonstration of code capability, the steady state TH analysis of a the WWER1000 core is compromised with Thermal-hydraulic analysis code (COBRA-EN). By thermal hydraulic parameters averaging Fuel Assembly-to-Fuel Assembly method, the one sixth (symmetry) of the Boushehr Nuclear Power Plant (BNPP) core with regular subchannels are modeled. Comparison between the results of the work and COBRA-EN demonstrates some advantages of the presented code. Using the code the thermal modeling of the fuel rods with considering the fission gas generation would be possible. In addition, this code is compatible with neutronic codes for coupling. This method is faster and more accurate for symmetrical simulation of the core with acceptable results.

Keywords: numerical method; thermal hydraulics; energy and power plant; nuclear energy

1. Introduction

The generation of electrical power with nuclear reactors needs the study of safety aspects in these systems (Guk and Kalkan 2015). In nuclear reactors, predicting the core criticality characteristics requires the simulation of the thermal-hydraulics and the neutronic as well as their feedbacks. For in-core thermal-hydraulic calculation, the subchannel method is preferred. The subchannel method is an interesting method for fluid flow simulations (Li *et al.* 2017, Mitsuyasu *et al.* 2017, Al-Waaly *et al.* 2017, Sharma *et al.* 2016, Cai *et al.* 2016, Sangeeta *et al.* 2013, Aghaie

---

et al. 2012a).

The quasi-static calculations like fuel management, burnup calculation, cross section generation, temperature-density dependent nuclear data processing, fuel rod design, shielding studies and safety are the most important application of this method. The subchannel model with high accuracy in calculations helps to achieve more accurate results in coupling schemes. Core calculation codes, almost for their thermal-hydraulic calculations utilize simple methods like single heated channel or interloping enthalpy rising methods. For instance, CORD-2 fuel management code (Trkov *et al.* 2008), DYNCO core complex calculation code and PARCS (Downar *et al.* 2006) with single phase thermal-hydraulic TH routine, are codes with standard simple core TH analysis. They applied special conditions and models for their specific calculation target. Pressure change, cross flow, turbulent mixing, and girder effects are not considered in these codes.

The COBRA-EN is a Thermal-hydraulic analysis code, (Aghaie *et al.* 2012b), is used for nuclear reactor core thermal-hydraulic calculations, in pressurized water reactors (PWRs) or boiling water reactors (BWRs). This code is an updated version of the COBRAIIIC and COBRA-IV-I codes. The COBRA-EN implements the subchannel method for its calculation. This code is generated for PWR reactors with squared fuel assemblies. Therefore, the hexagonal geometry of the WWER1000 and fuel pellets with central holes could not be modeled in this code and the gap model in does not have enough adaptability with WWER1000 reports.

This work has special applications to fulfill some above-mentioned disadvantages. As seen in recent researches the enhanced thermal hydraulic code for some calculation is needful. Recent research papers on WWER type core explicated this object. The WIMS-CITATION and COBRA-EN codes were coupled (Safaei *et al.* 2010) to investigate thermal hydraulic analysis of WWER1000 core. The COBRA-EN, WIMS and CITATION codes were coupled for steady state calculations in VVR-S analysis (Zare *et al.* 2010).

In the enhanced subchannel code by using the equations of the flow field in triangle subchannels, TH data were analyzed. The cylindrical heat transfer equation with finite difference and finite element solvers was solved and the central hole in fuel pellet was considered. By using the presented coupled models of the gap, the Calza-Bini with ORIGEN2.1 (Yakubu *et al.* 2015), temperature-burnup dependent property of gap was considered. By averaging FA to FA method, the one sixth of Boushehr core with regular subchannels is modeled. Finally, code results were compared with the manual implementation of WWER1000 model to COBRA-EN code and acceptable results are achieved.

2. Conservation equations for modeling

The general format of flow field equations in subchannel analysis is shown in Eqs. (1)-(4) (Tyurina *et al.* 2015). The mass, energy, axial momentum and lateral momentum conservations are desired equations. The heat transfer equation in cylindrical coordinate is added to these equations (Eq. (5)). In this work with an iterative method, mentioned equations are solved, numerically.

$$A_i \frac{\partial}{\partial t}\langle \rho_i \rangle + \frac{\Delta m_i}{\Delta z} = -\sum_{j=1}^{J} W_{ij} \tag{1}$$

$$A_i \frac{\partial}{\partial t} \left[\langle \rho h \rangle_i \right] + \frac{\Delta}{\Delta z} \left[\dot{m}_i h_i \right] = \langle q_i' \rangle_{rb} - \sum_{j=1}^{J} W_{ij}^{*H} \left[h_i - h_j \right] - \sum_{j=1}^{J} W_{ij} \{ h^* \} + A_i \left\langle \frac{Dp_i}{Dt} \right\rangle \quad (2)$$

$$\frac{\partial}{\partial t} \langle \dot{m}_i \rangle + \sum_{j=1}^{J} W_{ij} \{ v_z^* \} + \frac{\Delta(\dot{m}_i v_{zi})}{\Delta z} = -A_i \langle \rho \rangle g_z - A_i \frac{\Delta \{ p \}}{\Delta z} - \sum_{j=1}^{J} W_{ij}^{*M} (v_{zi} - v_{zj}) - \left\{ \frac{F_{iz}}{\Delta z} \right\} \quad (3)$$

$$\frac{\partial}{\partial t} \langle W_{ij}^x \rangle + \frac{\Delta}{\Delta z} (W_{ij}^x \{ v_z \}) = -\frac{s_{ij}^y}{l} (\Delta \{ p \}) - \left\{ \frac{F_{ix}}{l \Delta z} \right\} \quad (4)$$

$$\frac{\partial^2 T}{\partial r^2} + \frac{1}{r} \frac{\partial T}{\partial r} + \frac{\partial^2 T}{\partial z^2} + \frac{q''}{k} = 0 \quad (5)$$

Fig. 1 shows the general flowchart for the solution of equations. First, the mesh regeneration routine is called. The coolant enthalpies are calculated from the energy conservation equations for the individual control volumes. The axial pressure gradients are calculated from a combined axial and transverse momentum equation (a direct solution method is used at each axial level). The crossflows in the lateral directions are calculated from the lateral momentum equation, knowing the axial pressure gradients and the axial mass flowrates are obtained from the mass continuity equation. From the enthalpy of each computational cell, the steam quality and then, through the quality/void correlation, the steam volume fraction (or void fraction) and the coolant density are computed. The solution is iterative because the unknowns are not advanced simultaneously, apart from the presence of non-linear terms.
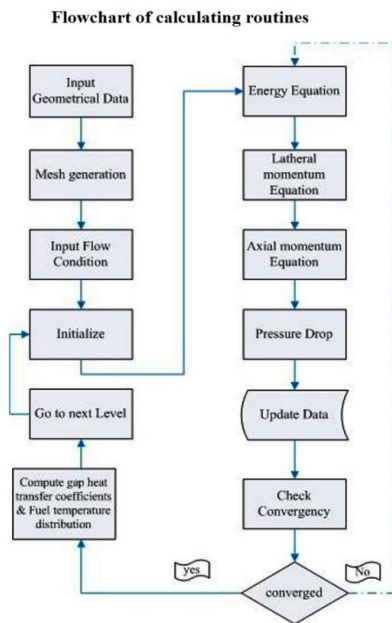

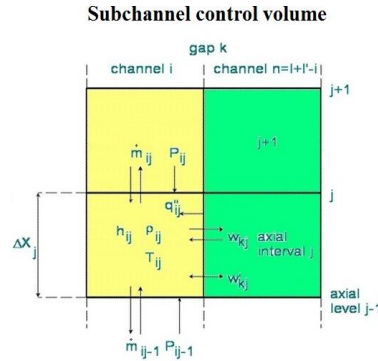Fig. 1 Flowchart of calculating routines

Fig. 2 Subchannel control volume

Fig. 2 shows the desired control volume for subchannels in axial and lateral directions. In solution routine, the thermal-hydraulic analysis is carried out in an array of parallel channels delimited by cylindrical fuel rods and open gaps. The axial direction is assumed parallel to the subchannels and oriented from the flow inlet to outlet. In linearized flow differential equations, the subchannels are divided into axial intervals by planes normal to the z-axis and not necessarily equally spaced. The volumes bounded by axial planes and channel lateral borders, i.e., gap open surfaces and rod solid walls, make up the three-dimensional grid of computational cells or control volumes for mass energy and lateral-axial momentum balance. Each cell is identified by a radial subchannel index i (i=1, 2, …, n) and by axial interval j.

The subchannel approximation of the flow equations assumes that the direction of a cross flow between two adjacent channels is dictated only by the correspondent gap orientation and is completely lost going from the gap to the interior of the confluence channel. This assumption also means that no fixed coordinate system is required in the radial plane but that only a local coordinate must be defined for each gap. The direction of a cross flow is the normal to the plane joining the centerlines of the fuel rods which delimit the corresponding gap.

3. Fuel model

The effects of the burnup and temperature on fuel-gap thermal properties show that application of the effective gap model is necessary. The Calza-Bini model (Eq. (6)) which coupled with Isotope Generation and Depletion Code (ORIGEN2.1) is prepared to help us for auxiliary calculations. The x_1, x_2, … are molar fraction of the Helium, Argon, Krypton, Xenon, H_2 and O_2. For computing, the molar fractions of gasses in gap region the Isotope Generation and Depletion Code (ORIGEN2.1) for each burnup was applied. Fig. 3 shows the gap thermal conductivity algorithm flow chart.

The gap conductance at the as-fabricated condition of the fuel can be modelled as due to conduction through an annular space as well as to radiation from the fuel. Where for an open gap

$$h_{gopen} = \frac{k_{gas}}{\delta_{eff}} + \frac{\sigma}{\frac{1}{\varepsilon_f} + \frac{1}{\varepsilon_c} - 1} \frac{T_{fo}^4 - T_{ci}^4}{T_{fo} - T_{ci}}$$

(6)

where h_{gopen} is heat transfer coefficient for an open gap; T_{fo} is fuel surface temperature, T_{ci} is clad inner surface temperature; k_{gas} is thermal conductivity of the gas, δ is effective gap width, σ is Stefan-Boltzmann constant, ε_f, ε_c are surface emissivity of the fuel and cladding, respectively.
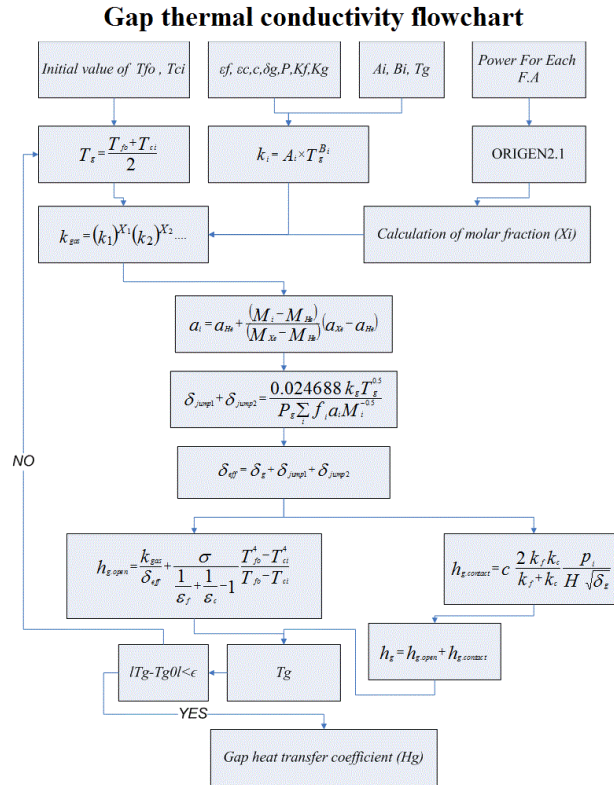

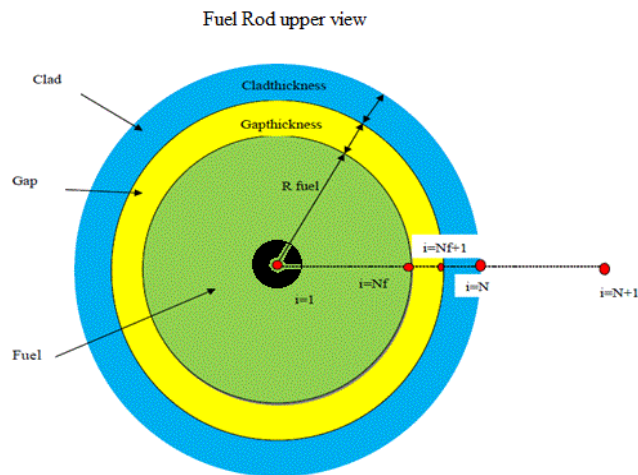Fig. 3 Gap thermal conductivity flowchart

Fig. 4 Fuel pellet with central hole

It should be noted that the effective gap width is larger than the real gap width because of the temperature discontinuities at the gas-solid surface. The temperature discontinuities arise near the surface owing to the small number of gas molecules present near the surface. At atmospheric pressure, $\delta_{jump1}+\delta_{jump2}$ were found to equal 10 μm in helium and 1 μm in xenon. The gas conductivity of a mixture of two gasses is given by

$$k_{gas} = (k_1)^{x_1}(k_2)^{x_2}... \tag{7}$$

When gap closure occurs because of fuel swelling and thermal expansion, the contact area with the cladding is proportional to the surface contact pressure between the fuel and cladding. (hg, contact) where C=a constant; Pi=surface contact pressure (psi) (usually calculated based on the relative thermal expansion of the fuel and the cladding, but ignoring the elastic deformation of the cladding); H=Meyer's hardness number of the softer material (typical values are, for steel, 13*10E4 psi and, for zircaloy, 14*10E4 psi); δg is mean thickness of the gas space (feet) (calculated based on the roughness of the materials in contact). The total gap conductance upon contact may be given by

$$h_g = h_{g,open} + h_{g,contact} \tag{8}$$

In presented algorithm for calculation of gap heat transfer coefficient, first, average gap temperature is obtained from fuel pellet outside and clad inside temperature. Then, by calculating other parameters, the gap heat transfer coefficient is achieved. The iteration loop will continue to satisfy convergence conditions.

In this work for fuel pellet with a central hole, temperature calculations routine is considered. The finite difference and finite element solver for accurate calculation are added. The isolated boundary (Eq. (9)) condition is considered for central hole side of fuel pellet (Fig. 4) by Eq. (9). In above equation, the r_{in} is the radius of central hole (Fig. 4). The central hole radius could be defined in the input by the user.

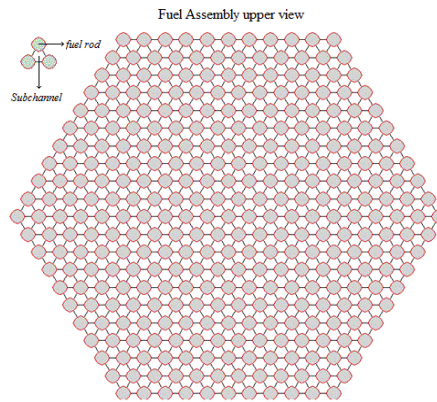$$\frac{\partial T}{\partial r}\left(r = r_{in}\right) = 0 \tag{9}$$
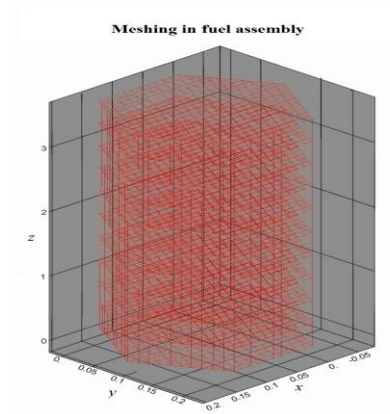

Fig. 5 Top view of subchannel generation

Fig. 6 3D view of subchannel for WWER1000 FA

4. Core mesh generation

The subchannel analysis needs all of the connection data for subchannels and rods. All of neighbor channels for each desired channel must be identified. Also, the connecting channels for each rod must be identified too. Cross flow, average coolant temperature and mixing calculation in subchannel analysis need above connecting data. The Delaunay triangulation 3D mesh generator is coupled to this work. In mathematics and computational geometry, a Delaunay triangulation for a set P of points in a plane is a triangulation DT(P) such that no point in P is inside the circumcircle of any triangle in DT(P). Delaunay triangulations maximize the minimum angle of all the angles of the triangles in the triangulation; Delaunay triangulations are often used to build meshes for space discretized solvers such as the finite element method and the finite volume method of physics simulation, because of the angle guarantee and because fast triangulation algorithms have been developed. Typically, the domain to be meshed is specified as a coarse simplicial complex; for the mesh to be numerically stable, it must be refined, for instance by using Ruppert's algorithm.

We developed our designed mesh generator for next works on CFD calculations but in this work, mesh generator generates only connection data for each channel and rod in the core model. Figs. 5 and 6 show the subchannels which were generated for desired core configuration.

Table 1 Main design parameters of WWER1000 NPP

Heat power, (MW)	3000
Primary circuit pressure, (MPa)	15.7
Secondary circuit pressure, (MPa)	6.3
Coolant temperature, (K)	290-330
Core length, (m)	3.53
Number of fuel rods	50,856
Core volume, (m^3)	14.8
Numbers of loops	4
Number of steam generators	4

Table 1 Continued

Heat exchanging surface, (m²)	6115
Water volume in primary circuit, (m³)	21
Number of pumps	4
Pressurizer volume, (m³)	79
Water volume in pressurizer, (m³)	55
Number of hydro-accumulators	4

Table 2 Fuel thermal conductivity with fuel temperature in the reactor core

Temperature (℃)	0	227	827	1227	1427	1627	2227	2827
Thermal conductivity(*w/m.k*)	8.15	6.7	3.75	2.8	2.5	2.4	2.5	3.5

Table 3 Cladding thermal conductivity with clad temperature in the reactor core

Temperature (℃)	0	200	300	400	500	600	1300	1800
Thermal conductivity(*W/m.k*)	17.2	19.3	20.1	20.5	20.9	21.8	31.2	33.4

Table 4 Axial power peaking factor coordinate from the core bottom

Kz factor PPF	5	15	25	35	45	55	65	75	85	95
	0.36	0.82	1.12	1.31	1.39	1.39	1.31	1.12	0.82	0.36

5. Subchannels simulation and results

The operating condition of the Boushehr WWER1000 core is presented in Table 1. The steady-state subchannel analysing results are present for this condition. In results, thermal properties are temperature dependent (see Tables 2 and 3). In these cases, the comparison of results with analytical calculations is carried out. The axial power peaking factors considered as Table 4 that is reported within the FSAR of Boushehr NPP. In addition, radial power peaking factor for the hot channel is 1.24.

Figs. 7 and 8 show axial temperature and enthalpy of coolant in the hot channel. These results are shown that temperature and enthalpy increment along the core in COBRA-EN and numerical code have an adequate acceptability.
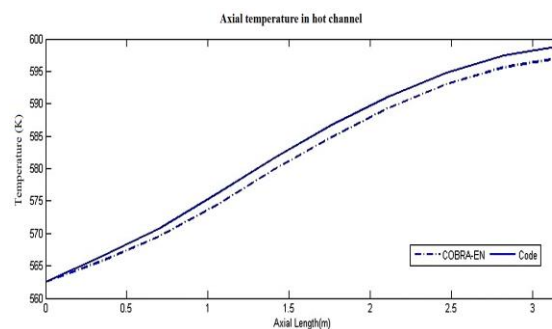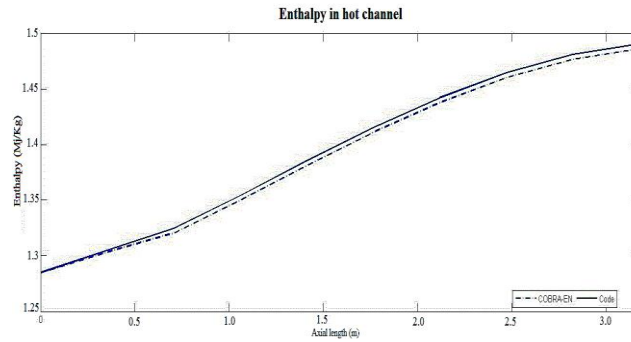

Fig. 7 Axial coolant temperature in hot channel

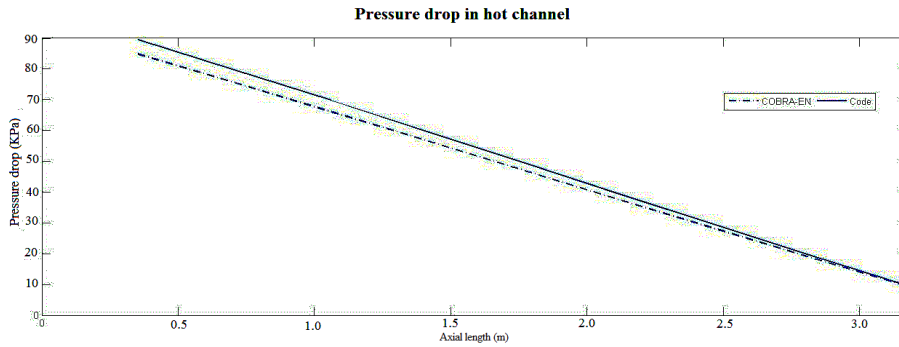Fig. 8 Axial coolant enthalpy rising in hot channel

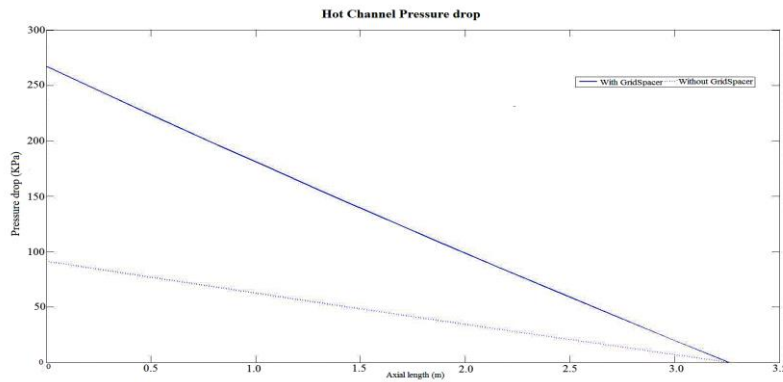Fig. 9 Axial pressure drop in hot channel

Fig. 10 Axial pressure drop in hot channel

In Fig. 9, axial pressure drop of the hot channel is depicted. Pressure drop in axial levels decreases because of coolant density reduction in upper levels of the core. This behaviour is seen in COBRA-EN and numerical code. The results in Figs. 7-9 are used as programming code verification.

The spacer-girder effect on pressure drop is shown in Fig. 10. Fig. 11 shows the gap heat transfer coefficient for desired fuel rods (27,105,277). As seen, with regard to fuel rods power peaking factor and neighbour channels the gap conductivity in desired fuel rods is different.

   Fig. 12 shows the radial fuel temperature profiles for the average rod. The finite difference and finite element radial temperature calculation compare with analytical calculations with constant thermal properties of fuel materials. Fig. 12 is reported for average fuel rod with solid fuel pellets and shows that numerical solvers acceptable accuracy. Due to low heat conduction coefficient of gap filled with fission gas (distance between fuel and clad), the temperature is decreasing strongly. Fig. 13 shows the radial temperature in average fuel rod, which contains fuel pellet with a central hole. As expected, the reduction of temperature for fuel pellet with a central hole is seen.
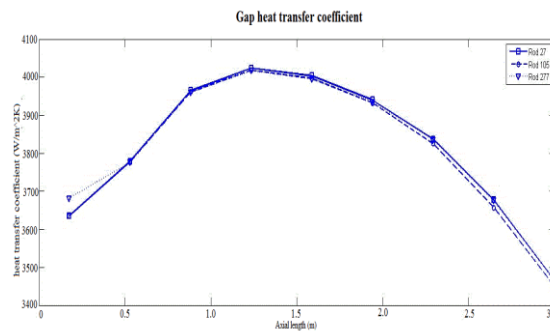
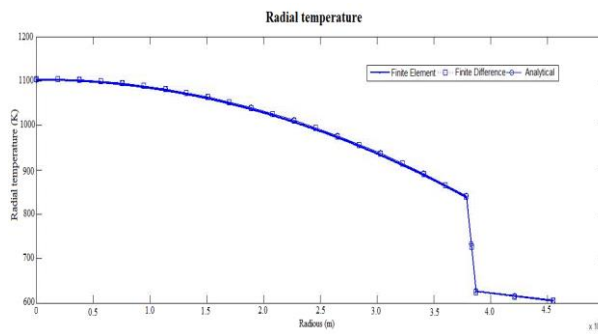Fig. 11 Gap thermal conductivity in desired fuel rods

Fig. 12 Radial fuel temperature profiles in finite difference, finite element and analytical methods for solid pellet
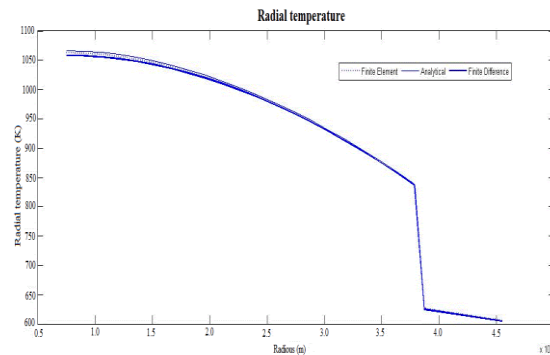

Fig. 13 Radial fuel temperature profiles in finite difference, finite element and analytical methods for pellet with central hole
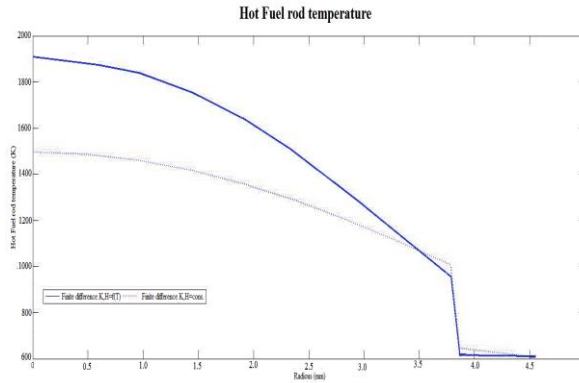
Fig. 14 Comparison of Radial temperature profile in solid fuel pellet with finite difference method for temperature dependent properties
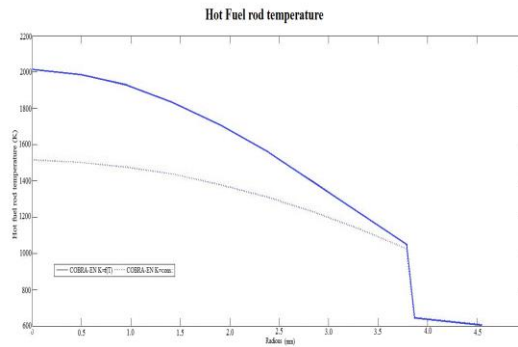

Fig. 15 Comparison of Radial temperature profile in solid fuel pellet with finite COBRA-EN for temperature dependent properties
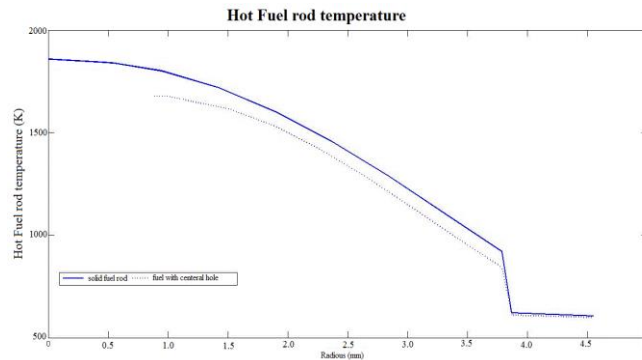

Fig. 16 Radial temperature profile in solid fuel pellet and fuel pellets with central hole

In Fig. 14, radial temperature of finite difference solver in temperature dependent and independent material properties is compromised. The reduction of thermal conductivity as temperature increment is caused radial temperature differences.

Fig. 15 shows the radial temperature of COBRA-EN in a temperature dependent and

independent material properties. The COBRA-EN dose not has acceptable adapted fuel, clad and gap thermal conductivity model. The radial temperature comparison in the hot channel for temperature-dependent fuel rod material in Fig. 15 shows some errors that occur in COBRA-EN calculations (The COBRA-EN results did not have acceptable fuel temperature profile that reported in Boushehr FSAR). The result of this work is clearly close to reported values in FSAR.

Fig. 16 shows the difference of fuel temperature profile in solid fuel pellet and central hole fuel pellets. The reduction of the maximum fuel temperature of fuel pellet is the advantage of a central hole in WWER type FAs.

Fig. 17 shows 3D axial coolant temperature in the hot channel. Fig. 18 shows the FA to FA averaging method. Considering this method, the core could be modelled in whole subchannels faster than others (one sixth of the core with about 16800 subchannels). In this way, all of the thermal hydraulic parameters in FA to FA are considered as average value.
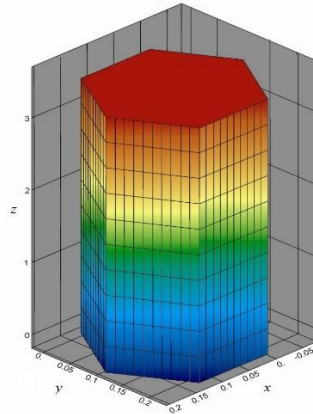

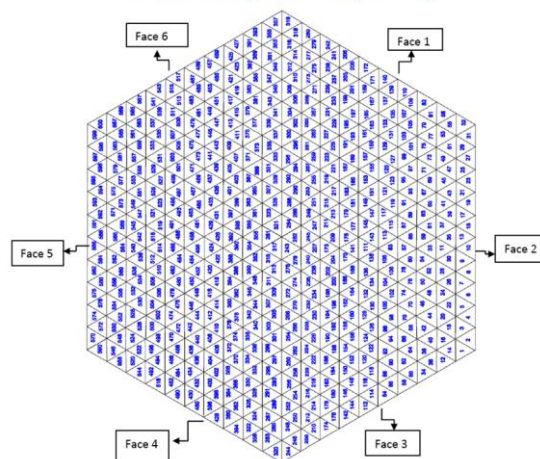Fig. 17 3D axial coolant temperature in a FA

Fig. 18 Fuel Assembly faces, Jointed Channels and FA configuration in one sixth of core (numbering of subchannels is shown)

6. Conclusions

Evaluation of results shows that a reliable numerical code for thermal-hydraulic calculation of the WWER type reactors with hexagonal FA configuration is obtained. The effective gap thermal conductivity (burnup-temperature) routine helps to achieve an accurate result for next calculations. The ORIGEN2.1 code for calculation of gap gasses concentration protected the Calza-Bini model and as shown previously, temperature profile especially across gap becomes more accurate. The automatic hexagonal FA configuration generation reduces time and errors in core definitions parameters. Faster and reliable generating of core configuration is the capability of this code. The possibility of radial and axial power peaking factor implementation is another useful capability that is introduced. Comparison between the results of code with COBRA-EN has demonstrated some advantages of the presented code. The possibility of fuel pellet with a central hole, temperature modelling, and gap model consideration are presented real calculation algorithms. The finite difference and finite element solvers for fuel rod temperature calculation reduces the calculative errors in comparison with other available codes. The code fulfils some disadvantages of COBRA-EN subchannel analysis, with adaptive routines applications. The averaging FA to FA method has acceptable results. Fig. 18 shows the FA to FA averaging method. This method is faster and helps to simulate symmetry core with acceptable results. The development of this code for PWR reactor core with rectangular is possible, easily.

Acknowledgments

References

Aghaie, M., Zolfaghari, A. and Minuchehr, A. (2012b), "Coupled neutronic thermal-hydraulic transient analysis of accidents in PWRs", *Annal. Nucl. Energy*, **50**, 158-166.

Aghaie, M., Zolfaghari, A., Minuchehr, A., Shirani, A. and Norouzi, A. (2012a), "Transient analysis of break below the grid in Tehran research reactor using the newly enhanced COBRA-EN code", *Annal. Nucl. Energy*, **49**, 1-11.

Al-Waaly, A.A., Paul, M.C. and Dobson, P. (2017), "Liquid cooling of non-uniform heat flux of a chip circuit by subchannels", *Appl. Therm. Eng*., **115**, 558-574.

Arshi, S. S., Mirvakili, S. M. and Faghihi, F. (2010), "Modified COBRA-EN code to investigate thermal-hydraulic analysis of the Iranian WWER1000 core", *Prog. Nucl. Energy*, **52**(6), 589-595.

Cai, R., Yue, N., Chen, R., Tian, W.X., Su, G.H. and Qiu, S.Z. (2016), "Development of a thermal-hydraulic subchannel analysis code for motion condition", *Prog. Nucl. Energy*, **93**, 165-176.

Deokattey, S., Bhanumurthy, K., Vijayan, P.K. and Dulera, I.V. (2013), "Hydrogen production using high temperature reactors: An overview", *Adv. Energy Res*., **1**(1), 13-33.

Downar, T., Xu, Y. and Kozlowski, T. (2006), *PARCS v2.7 U.S. NRC Core Neutronics Simulator USER MANUAL August, 2006*, School of Nuclear Engineering, Purdue University, West Lafayette, Indiana, U.S.A.

Guk, E. and Kalkan, N. (2015), "The importance of nuclear energy for the expansion of world", *Adv. Energy Res*., **3**(2), 71-80.

Ibrahim, Y.V., Adeleye, M.O., Njinga, R.L., Odoi, H.C. and Jonah, S.A. (2015), "Prompt neutron lifetime

calculations for the NIRR-1 reactor", *Adv. Energy Res.*, **3**(2), 125-131.

Li, R., Chen, X. N., Andriolo, L. and Rineiski, A. (2017), "3D numerical study of LBE-cooled fuel assembly in MYRRHA using SIMMER-IV code", *Annal. Nucl. Energy*, **104**, 45-52.

Mitsuyasu, T., Aoyama, M. and Yamamoto, A. (2017), "A coupling model for the two-stage core calculation method with subchannel analysis for boiling water reactors", *Annal. Nucl. Energy*, **102**, 77-84.

Sharma, M.P. and Nayak, A.K. (2016), "Experimental investigation of two phase turbulent mixing rate under bubbly flow regime in simulated subchannels of a natural circulation pressure tube type BWR", *Exp. Therm. Fluid Sci.*, **76**, 228-237.

Trkov, A., Ravnik , M., Kromar, M., Slavic, S., Mele, I., Zeleznik, N. and Zefran, B. (2008), C*ORD-2 Core Design System for PWR Type Reactors*, Joˇzef Stefan Institute, Ljubljana, Slovenia.

Tyurina, E.A. and Mednikov, A.S. (2015), "Energy efficiency analyses of combined-cycle plant", *Adv. Energy Res.*, **3**(4), 195-203.

USHEHR WWER1000 Reactor (2007), *Final Safety Analysis Report (FSAR)*, Ministry of Russian Federation of Atomic Energy (Atomenergoproekt), Moscow IPPE, Mathematical department DynCo code.

Zare, N., Fadaei, A.H., Rahgoshay, M., Fadaei, M.M. and Kia, S. (2010), "Introducing and validating a new method for coupling neutronic and thermal-hydraulic calculations", *Nucl. Eng. Des.*, **240**(11), 3727-3739.

CC

Nomenclature

A	Axial flow area (m^2)
h_{gap}	Gap conductance (w/m²c)
R	Radius(m)
$\dot{m}$	Axial mass flowrate (kg/s)
t	Time(s)
z	Axial direction(m)
w	Crossflow rate (kg/m/s)
h	Flowing enthalpy (kJ/kg)
g	Gravitational acceleration (m/s^2)
P	Pressure (N/m^2)
i	Channel index
j	Index of axial level
V_z^*	mass flux in z direction

h	Heat transfer coefficient (w/m^2. s)
k	Thermal conductivity (w/m K)
$F_{iz}/\Delta z$	Averaged force per unit length of the fluid
$s^y{}_{ij}$	Gap space between channel i, i+1
L	Length (m)
T	Temperature ($^\circ$C)
$\dot{q}$	Linear power generated in a rod (w/m)

Greek letters

ρ	Density (kg/m^3)

Subscripts

WWER	Water-cooled water-moderated reactor